Separation and Purification Technology 360 (2025) 130869

Contents lists available at ScienceDirect

Separation and Purification Technology

journal homepage: www.elsevier.com/locate/seppur

Dual-stage vacuum pressure swing adsorption for green hydrogen recovery from natural gas grids

Lucas F.A.S. Zafanelli [a,b,c,*], Ezzeldin Aly [a], Adriano Henrique [a], Alírio E. Rodrigues [b,c], José A.C. Silva [a,*]

[a] CIMO, LA SusTEC, Instituto Politécnico de Bragança, Campus Santa Apolónia, 5300-253 Bragança, Portugal
[b] LSRE-LCM – Laboratory of Separation Reaction Engineering – Laboratory of Catalysis Materials, Faculty of Engineering, University of Porto, Rua Dr. Roberto Frias, 4200-465 Porto, Portugal
[c] ALiCE – Associate Laboratory in Chemical Engineering, Faculty of Engineering, University of Porto, Rua Dr. Roberto Frias, 4200-465 Porto, Portugal

ARTICLE INFO

Editor name: Z Bao

Keywords:
Dual-stage vacuum pressure swing adsorption
Green hydrogen
Hydrogen separation
Hydrogen recovery
Natural gas pipelines
Fuel cell grade hydrogen
Aspen adsorption

ABSTRACT

Purification of green hydrogen (GH) from natural gas grids (NGG) can be expensive and challenging through a single-step Pressure Swing Adsorption (PSA) process due to the low H_2 concentration in the grid (<20 % v/v). Herein, we report for the first time the design of a dual-stage vacuum pressure swing adsorption process (DS-VPSA) to purify H_2 blended in NGG with a synergy action of two types of adsorbents: a Carbon Molecular Sieve 3K-172 (CMS) in stage 1 and zeolite 13X in stage 2. In Stage 1, the CMS kinetically separates H_2 from CH_4, pre-concentrating H_2 from 20 % to over 50–60 % (v/v), followed by Stage 2, where a thermodynamic separation with zeolite 13X achieves a final product with a high H_2 purity content (>99 % v/v). A mathematical model is developed in Aspen adsorption, where numerical simulations are performed to establish the best operating conditions of the global DS-VPSA. A parametric study is also conducted to optimize performance parameters such as recovery, purity, productivity, and specific energy. The results indicate that it is possible to achieve a final H_2 product with a purity of 99.97 % (fuel cell grade), a recovery of 67 %, and productivity of $1.60x10^{-2}$ kg_{H2}/kg_{ads}/hr, and a total specific energy consumption of 10.06 MJ/kg_{H2}, which is a significant achievement reported so far.

1. Introduction

A shift to renewable energy sources is crucial to mitigate climate change. According to the Intergovernmental Panel on Climate Change (IPCC) report, in 2019, the combined energy supply, industry, and transport sectors represented 73 % of the total net anthropogenic emissions, which means approximately 42.7 $GtCO_2$ was released into the atmosphere by these sectors [1]. The European Union (EU) has committed to reducing greenhouse gas (GHG) emissions by 55 % and aims to become the first climate-neutral continent by 2050. To achieve this goal, substantial investments are being made in projects designed to advance climate neutrality.

Green Hydrogen (GH), produced from the electrolysis of water, has the potential to play a significant role in reducing CO_2 emissions from fossil fuel systems. GH can serve as an intersectoral carrier by storing and utilizing intermittent renewable energy sources (such as wind and solar) for later use in the energy supply, industry, and transport sectors [2]. In the EU (+ United Kingdom), it is estimated that at least 84 regions have 50 % more renewable energy potential than is needed to cover the total electricity demand and current water electrolysis [3]. This surplus can be used to produce GH, which can then be transported throughout the EU by connecting it to the natural gas grid (NGG). The co-transport of GH in the existing NGG is an interesting alternative for cost-effective transportation, eliminating or reducing the need for extensive infrastructure investments [2,4,5]. Nevertheless, when GH is blended into the NGG, it is necessary to recover and purify it to a purity level according to the quality requirements of different end-users. For example, the purity level required for fuel cell applications is 99.97 %, and combustion applications must be higher than 98 % [6,7]. One challenge associated with separating and purifying GH blended in NGG is the low H_2 feed concentration (<20 %) [6], which is significantly lower than that required for traditional H_2 adsorption purification processes, for example, H_2 produced from steam methane reforming (>70 %) [8,9].

Pressure swing adsorption (PSA) and vacuum pressure swing adsorption (VPSA) are well-established processes for H_2 purification due to their energy efficiency, low cost, ease of operation, and design flexibility. In this view, several works in the literature address the

* Corresponding authors.
E-mail addresses: zafanelli@ipb.pt (L.F.A.S. Zafanelli), jsilva@ipb.pt (J.A.C. Silva).

https://doi.org/10.1016/j.seppur.2024.130869
Received 30 September 2024; Received in revised form 12 November 2024; Accepted 30 November 2024
Available online 2 December 2024

Nomenclature

a_p	Specific area of the pellet (m^{-1})
a_c	Specific area of the column (m^{-1})
b_i	Adsorption equilibrium constant of component i (bar^{-1})
$b_{\infty,i}$	Pre-exponential factor of the affinity constant at infinite temperature of component i (bar^{-1})
C	Total gas concentration (mol/m^{-3})
C_f	Feed gas concentration (mol/m^{-3})
C_{pg}	Heat capacity of gas ($J/mol\ K^{-1}$)
C_{ps}	Adsorbent specific heat capacity ($J/mol\ K^{-1}$)
d_b	Beads diameter (m)
d_c	Column diameter (m)
D_{ax}	Axial mass dispersion coefficient (m^2/s)
D_m	Molecular diffusivity (m^2/s)
D_p	Macropore diffusion coefficient (m^2/s)
D_c	Micropore diffusion coefficient (m^2/s)
F	Total molar flux ($mol\ m^{-2}\ s^{-1}$)
h_w	Constant heat transfer between gas and wall ($W\ m^{-2}\ K^{-1}$)
h_p	Film heat transfer coefficient ($W\ m^{-2}\ K^{-1}$)
k_{mic}	Micropore constant coefficient (s^{-1})
k_{mac}	Macropore constant coefficient (s^{-1})
K_p	Darcy's Law coefficient (−)
K_{ax}	Effective axial bed thermal conductivity ($W\ m^{-1}\ K^{-1}$)
K_s	Adsorbent thermal conductivity ($W\ m^{-1}\ K^{-1}$)
L_c	Length of column (m)
MW_i	Molecular weight of component i ($kg\ kmol^{-1}$)
m_{ads}	Mass of adsorbent (kg)
p_i	Partial pressure of component i (bar)
P	Total pressure of column (bar)
$\overline{q}_i$	Average adsorbed phase concentration of component i ($mol\ kg^{-1}$)
q^*	Equilibrium adsorbed concentration of component ($mol\ kg^{-1}$)
q_m	Maximum adsorbed phase concentration ($mol\ kg^{-1}$)
R	Universal gas constant ($J/mol\ K^{-1}$)
R_p	Adsorbent particle radius (m)
r_c	Crystal radius (m)
t	Time (s)
v_i	Interstitial velocity (m/s)
$v = v_i\varepsilon_b$	Superficial velocity (m/s)
y_i	Molar fraction of component i (−)
z	Axial coordinate in bed (m)

Greek letters

ΔH_i	Heat adsorption of species i ($J{\cdot}mol^{-1}$)
ΔH_{st}	Isosteric heat adsorption ($J{\cdot}mol^{-1}$)
ε_b	Bed porosity
ε_p	Particle porosity
ρ_p	Solid Density ($kg{\cdot}m^{-3}$)
ρ_s	Apparent adsorbent density ($kg{\cdot}m^{-3}$)
ρ_b	Bulk density ($kg{\cdot}m^{-3}$)

purification of H_2 from concentrations higher than 50 %. For example, the H_2 production and purification from steam methane reforming [9,10], ethanol reforming [11,12], methanol-steam reforming [13], coke oven [14], raw biogas [15], and recovery of H_2 from ammonia plants [16]. In these processes, adsorbents such as zeolite 5A, 13X, activated carbon, and alumina are used to adsorb CH_4 and low-concentration impurities such as CO_2, N_2, and CO and separate them from H_2, which is practically inert. The adsorbents mentioned have a very low affinity to H_2, which makes it relatively easy to concentrate during the PSA/VPSA feed step. However, when the concentration of H_2 is low in the feed (<20 %), conventional PSA/VPSA processes are energetically inefficient to produce a high-purity H_2 [17].

Few works in the literature have addressed the recovery and purification of H_2 from mixtures where it is at a low concentration (<20 % v/v) using conventional H_2 purification processes [4,5,7,18–23]. These works studied the recovery of H_2 from the NGG, with the H_2 concentration varying from 1 % to 30 %. To our knowledge, only two works have proposed processes to recover H_2 from the NGG by employing selective adsorbents for H_2. In the first work, Yang *et al.* [6] used zeolite 3A to capture H_2 from natural gas grids. Zeolite 3A has a very narrow pore size of around 3 Å, which blocks the CH_4 entering as it has a kinetic diameter of 3.80 Å while allowing the entering of H_2, whose kinetic diameter is 2.89 Å. The authors designed and customized the VPSA cycles to capture H_2, from an initial concentration of 5 to 15 %, at pressures 10, 30, and 50 bar and room temperature. Their main objective was not to purify H_2 but to increase the CH_4 concentration from 85-95 % to over 99 % to meet the industry requirement. In the second work, Zafanelli *et al.* [24] addressed the recovery and purification of H_2 from NGG using a carbon molecular sieve (CMS) 3K-172 adsorbent, which kinetically separates H_2 from CH_4. It is well known that methane has a limited diffusion into the CMS, which makes it possible to kinetically separate CH_4 from lower molecules such as CO_2, N_2, and H_2 [24–27]. The authors developed a VPSA process that effectively concentrates H_2 from 20 to 68 % with a recovery rate of up to 92 % using the CMS-3K-172. Although the VPSA-CMS process cannot achieve high H_2 purity on its own, it can serve as a pre-enrichment step, followed by a conventional PSA process to produce the desired high-purity H_2 product. This integration can potentially increase the purity of H_2 for fuel cell applications and minimize the energy expended in the process.

Hybrid (membrane-PSA) or two-stage (PSA-PSA/VSA-VSA) processes have been introduced previously, and studies on recovering and purifying H_2 from natural gas grids exist in the literature. Liemberger *et al.* [18] proposed a hybrid approach combining membrane technology and PSA to purify hydrogen for fuel-cell-grade purity. They tested different pressures and stage-cut values for membrane separation, optimizing conditions at 6 bar and 20 % H_2 concentration in the permeate. This permeate was then fed into the PSA process using activated carbon as the adsorbent, which adsorbs CH_4 preferentially than H_2. The PSA achieved over 99 % hydrogen purity with a recovery rate of at least 60 %. Dehdari *et al.* [22] demonstrate that a double-stage VSA can reduce energy consumption compared to a single stage for purifying H_2 from natural gas grids. The authors proposed the double-stage VSA filled with commercial activated carbon, which adsorbs CH_4 preferentially than H_2. After validating the simulation results with experimental data, they used Aspen Adsorption software to design a five-bed, double VSA system at an industrial scale. The results indicate that achieving over 99 % hydrogen purity and 82 % recovery at a 110 kPa feed pressure is possible.

In this study, we have developed a new dual-stage VPSA process to separate and produce high-purity GH blended in NGG. The innovation of this work lies in the synergistic action of two types of adsorbents used in each stage. Stage 1 consists of a VPSA-CMS process using the adsorbent CMS-3K-172 that kinetically separates CH_4 from H_2, intending to pre-concentrate H_2 from 20 % to 50 %. The pre-enriched H_2 is then fed into Stage 2, where a conventional VPSA-13X process using the benchmark zeolite 13X (13XBFK) enriches H_2 from 50 % to 99.97 %. A mathematical model was developed and simulated using the Aspen Adsorption software to evaluate the performance of the dual-stage VPSA process. A parametric study is performed to establish the best operating conditions, studying the effect of process variables such as step time,

vacuum pressure, and number of pressure equalization steps in the global performance of the dual-stage VPSA process. Also, performance parameters such as productivity, H_2 purity, H_2 recovery, and specific energy consumption are calculated.

2. Experimental and Methods

2.1. Dual-stage cycle design

The design of the dual-stage VPSA process for the H_2/CH_4 separation has been developed by combining elementary steps necessary to attain a high purity and recovery of either H_2 or CH_4. These include adsorption (ADS), pressure equalization (PE) that refers to depressurization pressure equalizations (DPEs) and pressurization pressure equalizations (PPEs), countercurrent vacuum blowdown (CVB), and pressurization with the light product (PLP) steps.

2.1.1. Stage 1 – VPSA filled with CMS-3K-172

The VPSA using CMS as an adsorbent was studied in our previous work [24]. However, a different step configuration was proposed in the present work, as shown in Fig. 1. Stage 1 consists of a VPSA filled with a carbon molecular sieve (CMS-3K-172), which kinetically separates H_2 from CH_4. The elementary steps used in Stage 1 are:

(1) Adsorption (ADS)
(2) Depressurization pressure equalization 1 (DPE1)
(3) Depressurization pressure equalization 2 (DPE2)
(4) Countercurrent vacuum blowdown (CVB)
(5) Pressurization pressure equalization 1 (PPE1)
(6) Pressurization pressure equalization 2 (PPE2)
(7) Pressurization with the light product (PLP)

In this way, CH_4 is produced in the ADS step, while H_2 is enriched in the CVB step. This cycle, shown in Fig. 1, consists of 7 steps combining the abovementioned steps. In the ADS step, H_2 is adsorbed while CH_4 is withdrawn and enriched at the top of the column. During DPE1 and DPE2 steps, the high-pressure column is partially depressurized to an intermediate pressure by connecting it to a low-pressure column using the top-top equalization strategy. The main goals of the DPE steps are to save energy and reduce the loss of the light product while increasing its recovery [28].

After that, the column is counter-currently depressurized to a vacuum pressure CVB step. In the CVB step, H_2 is enriched from the column bottom and sent to a storage tank connected to stage 2; simultaneously, the column is regenerated to start a new cycle. Following the CVB step, during PPE1 and PPE2, the column is partially re-pressurized to an intermediate pressure by receiving material from a high-pressure column. The PPE steps undergo the DPE steps. Finally, during the PLP step, the column is pressurized to the feed pressure using part of the CH_4 produced in the ADS step, which is the light product of stage 1.

The advantage of using CMS-3K-172 in the first stage is that CH_4, which has a higher concentration in the feed (>80 %), can be produced during the feed step, while H_2, which has a lower concentration in the feed (<20 %), is retained in the column and produced when the column is regenerated. A significant amount of CH_4 produced in the feed step can be sent directly to the NGG at 30 bar without the need for compressing. Also, since the H_2 isotherm on CMS is almost linear [24], the column's regeneration can be done easily (less energy spent). If, otherwise, we use a PSA with 13X in the first stage, 80 % of the feed will be retained in the adsorbent at 30 bar, with a high demand of energy to desorb it at atmospheric conditions. Thereafter, the tail gas must be recompressed to 30 bar or 4 bar to be injected into the grids.

2.1.2. Stage 2 – VPSA filled with 13X

Stage 2 consists of a VPSA process with a column filled with binder-free zeolite 13X, which preferentially adsorbs CH_4 over H_2, which is the opposite of what happens in stage 1. Thus, H_2 is produced in the ADS step, while CH_4 is enriched in the CVB step. This cycle, shown in Fig. 1,

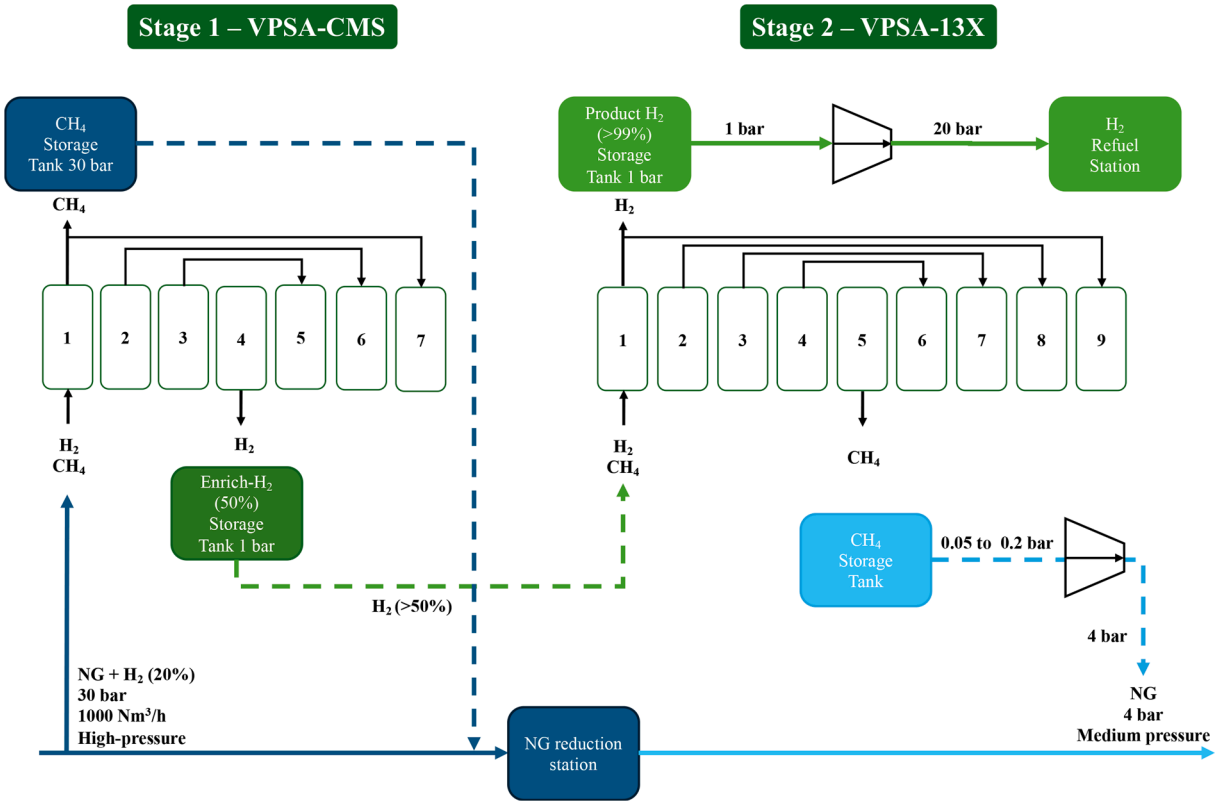

Fig. 1. Dual-stage vacuum pressure swing adsorption process flow diagram for the H_2 recovery from natural gas grids.

consists of 9 steps as follows:

(1) Adsorption (ADS)
(2) Depressurization pressure equalization 1 (DPE1)
(3) Depressurization pressure equalization 2 (DPE2)
(4) Depressurization pressure equalization 3 (DPE3)
(5) Countercurrent vacuum blowdown (CVB)
(6) Pressurization pressure equalization 1 (PPE1)
(7) Pressurization pressure equalization 2 (PPE2)
(8) Pressurization pressure equalization 3 (PPE3)
(9) Pressurization with the light product (PLP)

The cycle configuration is practically the same as stage 1, differing only that in stage 2, two additional steps, one DPE3 and one PPE3 step, were added to the cycle to ensure a high H_2 recovery. H_2 is the light product of the stage 2.

2.2. Process performance metrics

Each stage performance was evaluated in terms of purity, recovery, productivity, and specific energy calculated according to the following equations after achieving cycle at cyclic steady state (CSS) for the heavy product *i* in each stage,

$$Purity_i(\%) = \frac{\int_0^{t_{vac}} y_i F_{vac} dt}{\int_0^{t_{vac}} F_{vac} dt} \times 100 \quad (1)$$

$$Recovery_i(\%) = \frac{\int_0^{t_{vac}} y_i F_{vac} dt}{\int_0^{t_{ads}} y_i F_{feed} dt} \times 100 \quad (2)$$

for the light product *j* in each stage,

$$Purity_j(\%) = \frac{\int_0^{t_{ads}} y_j F_{prod} dt}{\int_0^{t_{ads}} F_{feed} dt} \times 100 \quad (3)$$

$$Recovery_j(\%) = \frac{\int_0^{t_{ads}} y_j F_{prod} dt - \int_0^{t_{PLP}} y_j F_{PLP} dt}{\int_0^{t_{ads}} y_j F_{feed} dt} \times 100 \quad (4)$$

where, *y* is the molar fraction of component *i* or *j*, F_{prod}, F_{PLP}, F_{feed}, and F_{vac} are the instantaneous gas flowrates of the product, pressurization with the light product, and feed and vacuum streams (STP condition), respectively; t_{vac} is the vacuum step time, t_{ads} is the adsorption step time, and t_{PLP} is the pressurization with the light product step time. In stage 1, H_2 is the heavy product *i*, and CH_4 is the light product *j*, and in stage 2, H_2 is the light product *j*, and CH_4 is the heavy product *i*.

H_2 and CH_4 productivities can be calculated according to equation (5),

$$Productivity\left(\frac{kg_i}{kg_{ads} hr}\right) = \frac{\int_0^{t_{ads}} y_i F_{feed} dt \times Recovery \times MW_i}{W_{ads} t_{cycle}} \quad (5)$$

Where MW_i is the molecular weight of component *i*, W_{ads} is the adsorbent weight, and t_{cycle} is the cycle time. The productivity is given in kilogram of H_2 or CH_4 (kg_i) per kilogram of adsorbent (kg_{ads}) per hour (*hr*).

The energy consumption in the dual-stage VPSA process is a critical indicator for evaluating separation performance when a vacuum is included. The typical pressure in the natural gas grid ranges from 1 to 120 bar, which can be categorized as follows: (i) transport level, which is between 70 and 120 bar, (ii) distribution level, ranging from 6 to 70 bar, and (iii) local distribution level, which is below 6 bar [4]. The dual-stage VPSA was designed for installation at a pressure reduction station (PRS) operating within a pressure range of 30 bar to 4 bar, typical of local natural gas grid (NGG) distribution levels [21]. In this configuration, the feed pressure from the NGG is sufficient to drive Stage 1 (30 bar), while Stage 2 operates at atmospheric pressure, eliminating the need for inlet gas compression in either stage. Additionally, the CH_4 produced in Stage 1 (30 bar) can be directly returned to the distribution level, and the tail gas from Stage 2 requires less energy for recompression to 4 bar before re-entering the grid at the local distribution pressure. Therefore, the energy consumption is required only in the vacuum step, and the specific energy can be evaluated by equation (6) [21],

$$Sp.energy\left(\frac{J}{kg_i}\right) = \frac{\int_0^{t_{vac}} \frac{l}{l-1} \frac{F_{vac} P_{vac}}{\eta} \left[\left(\frac{P_{atm}}{P_{vac}}\right)^{\frac{l-1}{l}} - 1\right] dt}{\int_0^{t_{ads}} y_i F_{feed} dt \times Recovery_i \times MW_i} \quad (6)$$

here, *l* is the ratio of heat capacities of the gas mixture at constant pressure and volume (C_p/C_v, which was assumed to be 1.3 for CH_4 and 1.4 for H_2). η is the vacuum pump efficiency assumed to be 0.7. F_{vac}, P_{vac}, and P_{atm} are the instantaneous volumetric gas flow rate, vacuum pressure, and atmospheric pressure, respectively.

2.3. Mathematical modeling and numerical method for the dual-stage VPSA

The dual-stage VPSA unit was modeled and simulated with the Aspen Adsorption numerical package.

Stage 1 model assumptions were already discussed in our previous work [24]. Briefly, the assumptions are:

- Ideal gas law as equation of state (EoS).
- A bi-linear driving force model (bi-LDF) model was used to evaluate the adsorption kinetics in the CMS-3K-172.
- Darcy's law was used to describe the pressure drop in the column.
- Axially dispersed plug flow was used.
- Langmuir isotherm model describes the H_2 adsorption on CMS-3K-172, while CH_4 is considered inert due to its strongly limited diffusion.
- The stage 1 VPSA operation system was considered isothermal due to the low H_2 heat of adsorption.
- The concentration, pressure, temperature, and velocity radial gradients were neglected.

Stage 2 mathematical model assumptions differ from Stage 1 only in the following considerations:

- Peng Robinson as EoS.
- The dual-site Langmuir isotherm model was used to describe the adsorption equilibrium of both H_2 and CH_4 on 13XBFK.
- The adsorption kinetics is predicted by a linear driving force model (LDF)
- Ergun equation was used to describe the pressure drop in the column.
- The Stage 2 VPSA operation system was considered adiabatic with gas and solid heat conduction.

The mathematical model equations and parameters, summarized in Tables S1 and S5 for Stage 1 and Tables S2 and S6 for Stage 2, were implemented in the Aspen Adsorption package, where the method of lines is used to solve numerically the set of coupled partial and algebraic differential equations [29]. The spatial derivatives were discretized by an upwind differencing scheme (UDS) into a uniform grid of 70 points. The boundary conditions for the dual-stage VPSA model are summarized in Table S3. To reduce the number of equations to be solved, a "Single Bed Approach" was used to decrease the computational time while obtaining accurate results at cyclic steady-state conditions for each stage [30]. In this approach, an interaction bed temporarily stores the effluent information such as pressure, temperature, flowrate, and composition from the depressurization pressure equalization steps. Then, it uses these data while the bed undergoes a pressurization pressure equalization step in a top-top equalization strategy.

2.4. Aspen adsorption flowsheet description and simulation conditions

A detailed description of each block of the simulation flowsheet is provided here. The flowsheet, with each block identified, is depicted in Fig. 2.

As mentioned, a "Single Bed Approach" was used to decrease the computational time. Thus, interaction units (IUs, shown in Fig. 2) store critical information from the bed, which is later playback when required according to the steps scheduled. In the flowsheet presented in Fig. 2, three IUs and their respective valves (VIUs) were used to perform the equalization steps. Two tank void blocks (Void1 and Void2) were used to consider the dead volume in pipes, valves, and connections at the inlet and outlet of the Bed block shown in Fig. 2. The Feed block, shown in Fig. 2, is used as an inlet boundary unit, where the stream composition, pressure, and temperature are specified.

The product blocks, Light_Product and Heavy_Product, act as outlet boundary units with constant pressures, which receive material from the adsorption bed (see Fig. 2). Eight valves were used to control the flowrate: Vfeed, VLP1, VLP2, VPLP, VHP, VIU1, VIU2, and VIU3. These valves can be set as fully open, fully closed, with a constant flowrate, and as a valve constant (CV), a function of pressure drop across the valve. The CV can be estimated according to the equations shown in the SI. A light product storage tank, Tank_LP, shown in Fig. 2, was used to store the light product and perform the pressurization with the light product later in the cycle. In the Bed block, shown in Fig. 2, the mathematical model is set according to the assumptions mentioned, and all the parameters are set, such as column dimensions, adsorbent properties, isotherm parameters model, sorption kinetic parameters, etc. Finally, the Cycle_Organizer block schedules the steps considering the interaction between the Bed and IUs. This flowsheet was used to simulate both stages.

The simulations were performed at a temperature of 195 K, and the feed gas flowrate, for stage 1, was 1000 Nm^3/hr. The lower temperature was used to increase each material's working capacity. The range of vacuum pressure was 0.2–0.8 bar in Stage 1 and 0.05–0.20 bar in Stage 2. Stage 2 target is to deliver H_2 at 99.97 % purity, so deeper vacuum values were tested to increase the working capacity towards CH_4, which results in a high purity of H_2 at the ADS step. Table 3 summarizes the simulation conditions and bed properties used in the work. The range of operating conditions in the performance analysis were defined based on previous simulations.

2.5. Materials

Carbon molecular sieve CMS-3K-172, kindly supplied by Osaka Gas Chemicals Co. (Japan), was used in stage 1, which kinetically separates CH_4 from H_2, as was shown in our previous work [24]. In stage 2, binder-free zeolite 13X (13XBFK), kindly supplied by Chemiewerk Bad Koestritz GmbH (Germany), was used due to its capacity to thermodynamically adsorb reasonable amounts of CH_4 and being practically inert to H_2 [23]. The adsorbent properties are summarized in Table 1. The adsorption isotherms of H_2 and CH_4 were measured experimentally in our previous works [23,24]. Langmuir and Dual-Site Langmuir isotherm models fit the experimental data. The isotherm parameters for H_2 and CH_4 on zeolite 13XBFK and CMS-3K-172 are summarized in Table 2 [23,24].

Table 1
Simulation conditions and column properties of the DS-VPSA.

Properties	Stage 1	Stage 2
Material	CMS-3K	Zeolite 13X
Adsorbent mass (kg)	67	413
L_c (m)	1.66	2.50
D_c (m)	0.30	0.60
V (m^3)	0.118	0.707
Bed porosity (–)	0.444	0.400
P_{ADS} (bar)	30	1
P_{VAC} (bar)	0.20–0.80	0.05–0.2
T (K)	195	195

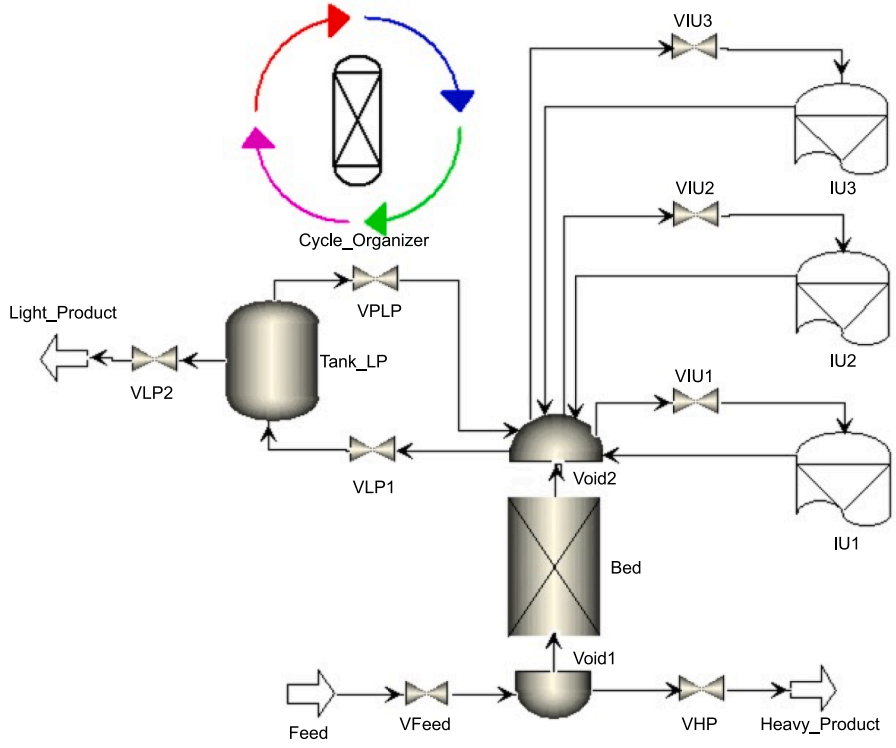

Fig. 2. Aspen Adsorption Flowsheet for simulating the DS-VPSA stages 1 and 2.

Table 2
Adsorbent materials properties.

Propreties	CMS-3K-172	13XBFK
Particle diameter (mm)	1.8	1.6–2.5
Particle length (mm)	1.18–2.8	–
Particle porosity (−)	0.31	0.40
Particle density (g/cm^3)	1.028	1.085
Adsorbent shape	cylindrical	beads

Table 3
Isotherm parameters for the sorption of H_2 and CH_4 on zeolite 13XBFK and H_2 on CMS-3K-172.

Species	q_m(mol kg^{-1})		b(bar^{-1})[a]		(ΔH_i)(kJ/mol)	
	q_{m1}	q_{m2}	b_1	b_2	$(\Delta H_i)_1$	$(\Delta H_i)_2$
13XBFK						
CH_4	2.13	5.12	0.41	8.04	−16.1	−18.0
H_2	12.65	–	0.016	–	−7.0	–
CMS-3K-172						
H_2	3.91	–	4.67×10^{-2}	–	−8.33	–

3. Results and discussion

3.1. Mathematical model validation

The mathematical model developed for simulating stages 1 and 2 was validated by reproducing the data results reported by Dehdari *et al.* [21]. The authors conducted a comprehensive study to assess the viability of a vacuum swing adsorption (VSA process for purifying H_2 from NGG at low pressure, where a four-bed VSA apparatus filled with Norit RB4-activated carbon was used to enrich H_2. The experiments were conducted with H_2 feed concentrations of 30 % and 50 %, balanced with CH_4, at a pressure of 102 kPa.

For the validation, the mathematical model was implemented in Aspen Adsorption with the data provided by the authors summarized in Table S4. First, we reproduce the simulation of the breakthrough curve experiment of CH_4/H_2 (30/70 %) on Norit RB4-activated carbon. Fig. S1A illustrates a good agreement between simulation and experimental data. After that, the mathematical model was adapted to simulate the VSA with 4-bed and 3-pressure equalization.

The model presented by Dehdari *et al.* [21] also includes an idle step (step where the column is closed in both in- and outlet). In this way, we have introduced the idle steps in our model to ensure that the reproduction of their data remains consistent. Figs. S1B and S1C illustrate the pressure and temperature profiles over one cycle at cyclic steady-state conditions. As illustrated in the Figs. S1B and S1C, the mathematical model developed in this study, accurately predicts the data reported by the authors. After validation, the model was used to simulate the process presented in this work.

3.2. Stage 1 VPSA performance analysis

The main objective of Stage 1 is to increase the H_2 concentration by up to 50 % and achieve the highest possible recovery rate. Thus, a parametric study was conducted in Stage 1 by varying the process variables, such as adsorption time (t_{ads}), vacuum pressure (P_{vac}), and the number of pressure equalization steps (PE). Each DPE, PPE, and PLP step lasts 5 s. The ADS step varies from 10 to 20 s, and the CVB step time equals the ADS step time. The CSS for stage 1 is achieved after more than 20 cycles. The main results achieved by the parametric studies for Stage 1 are summarized in Table 4. For example, run 7, in Table 4, shows that Stage 1 can increase the H_2 concentration from 20 % to 50 %, with a recovery of up to 93 %. We conducted simulation runs without vacuum pressure, which led to a significant decrease in recovery rates. For instance, during the simulation of run 7, we set the low pressure at 1 bar instead of 0.20 bar and the H_2 recovery drops from 93 % to 86 % and the H_2 purity from 50 % to 47 %. As a result, we have decided to keep the desorption pressure within the vacuum level range of 0.20–0.80 bar for the sensitivity analysis.

Fig. 3 shows the simulation results for H_2 purity and recovery with

Table 4
Operating conditions and process performance of the Stage 1 DS-VPSA.

Run	PE	t_{ads} (s)	P_{vac} (bar)	H_2 purity (%)	H_2 recovery (%)	CH_4 purity (%)	CH_4 recovery (%)	Sp. Energy (MJ/kg$_{H2}$)	Productivity (kg$_{H2}$/kg$_{ads}$/hr)
1	1	10	0.2	41.80	97.46	99.71	29.26	0.633	1.12×10^{-1}
2	1	15	0.2	47.65	91.18	98.85	47.27	0.699	1.21×10^{-1}
3	1	20	0.2	50.27	81.45	96.89	58.02	0.633	1.19×10^{-1}
4	1	10	0.8	41.48	94.91	99.47	30.57	0.021	1.07×10^{-1}
5	1	15	0.8	45.99	85.42	98.16	48.48	0.019	1.11×10^{-1}
6	1	20	0.8	47.56	74.06	96.27	59.31	0.017	1.06×10^{-1}
7	2	10	0.2	50.01	93.22	98.43	49.41	0.786	7.30×10^{-2}
8	2	15	0.2	55.71	81.21	97.51	65.15	0.644	7.74×10^{-2}
9	2	20	0.2	57.19	69.74	95.57	74.41	0.484	7.50×10^{-2}
10	2	10	0.8	48.79	89.10	98.48	50.73	0.023	6.87×10^{-2}
11	2	15	0.8	53.05	74.92	96.77	66.15	0.021	7.01×10^{-2}
12	2	20	0.8	54.47	62.86	94.81	74.66	0.022	6.70×10^{-2}
13	3	10	0.2	55.87	89.25	98.56	61.44	0.900	5.37×10^{-2}
14	3	15	0.2	59.98	73.55	96.73	74.80	0.334	5.53×10^{-2}
15	3	20	0.2	60.94	60.02	94.63	81.89	0.250	5.26×10^{-2}
16	3	10	0.8	54.28	84.23	98.18	62.43	0.023	5.01×10^{-2}
17	3	15	0.8	57.53	67.90	96.19	75.51	0.021	5.05×10^{-2}
18	3	20	0.8	56.13	58.17	94.14	85.94	0.020	5.05×10^{-2}
19	1	10	0.1	41.74	97.60	99.73	28.81	1.101	1.12×10^{-1}
20	1	10	0.4	41.68	96.57	99.63	29.58	0.225	1.10×10^{-1}
21	1	10	0.6	41.58	95.72	99.55	30.12	0.084	1.09×10^{-1}
22	2	10	0.4	49.71	91.73	98.73	50.14	0.302	7.14×10^{-2}
23	2	10	0.6	49.32	90.14	98.60	50.81	0.092	6.98×10^{-2}
24	3	10	0.4	55.66	88.41	98.50	61.68	0.387	5.31×10^{-2}
25	3	10	0.6	54.97	86.21	98.34	61.93	0.134	5.16×10^{-2}
26	3	15	0.6	59.11	71.62	96.54	74.99	0.132	4.98×10^{-2}
27	3	20	0.6	59.69	57.84	94.38	82.08	0.096	4.41×10^{-2}
28	3	10	0.8	54.28	84.31	98.18	62.42	0.040	5.01×10^{-2}
29	3	15	0.8	57.83	68.81	96.26	75.32	0.075	4.76×10^{-2}
30	3	20	0.8	58.83	56.31	94.20	82.22	0.068	4.28×10^{-2}

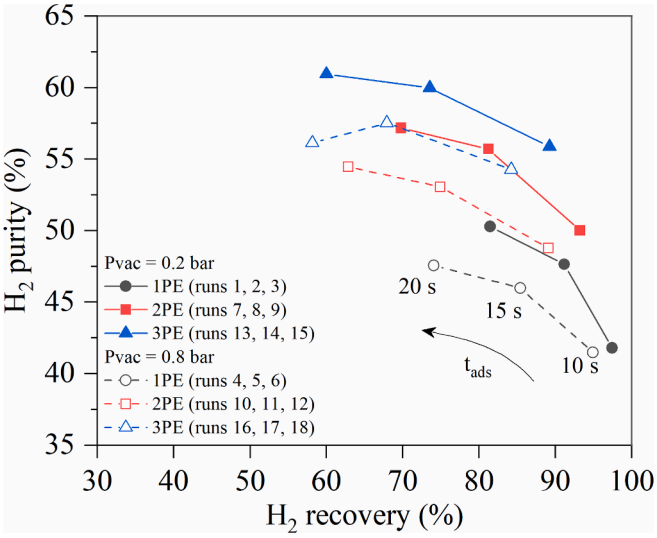

Fig. 3. The trade-off between H_2 purity and recovery for Stage 1 for different P_{vac}, t_{ads}, and numbers of PE.

different values of P_{vac} and t_{ads}, and the number of pressure equalization (PE) used in the cycle. As more PE steps are used in the cycle, the purity increases while the recovery decreases. This is expected because some H_2 from the high-pressure column flows to the low-pressure column during the PE steps, leading to less H_2 in the column available for recovery during the vacuum step. At the same time, CH_4, in the gas phase, is sent to the low-pressure column during the PE steps, which leads to an increase in H_2 purity in the vacuum step. It is worth mentioning that in stage 1, H_2 is the heavy component. As low as the P_{vac} used in the cycle, the H_2 purity and recovery increase. For example, by comparing runs 10 (P_{vac} = 0.8 bar) and 7 (P_{vac} = 0.2 bar), the H_2 purity and recovery increase from 48.79 to 50.01 % and 89.10 to 93.22 %, respectively (see runs in Table 4 and Fig. 3). At the same vacuum pressure and PE number step, H_2 purity increases while H_2 recovery decreases by increasing the adsorption time (t_{ads}). For example, using 2 PE and P_{vac} = 0.2 bar, the H_2 purity increases from 50.01 % (run 7) to 57.19 % (run 9), and H_2 recovery decreases from 93.22 % (run 7) to 69.74 % (run 9) by increasing the adsorption time from 10 to 20 s (see Table 4). As the adsorption time is longer, more H_2 is introduced to the bed, and its front is moved to the bed outlet, leading to a lower recovery in the CVB step. Otherwise, the H_2 front is also responsible for displacing CH_4 out of the bed, which leads to higher H_2 purity in the CVB step. The main goal of Stage 1 is to pre-enrich H_2 to be further purified in Stage 2. Therefore, to avoid H_2 losses, the adsorption time was fixed at 10 s for the following studies.

Fig. 4 illustrates the impact of the number of PE steps and P_{vac} values on H_2 recovery and purity. Low P_{vac} values result in higher H_2 recovery (Fig. 4a). Notably, H_2 purity appears unaffected by P_{vac} when 1 PE is utilized. However, with 2 PE and 3 PE, H_2 purity decreases slightly as P_{vac} increases. H_2 recovery and purity show opposite trends as the PE step numbers are increased. The higher the number of PE used in the cycle, the higher the H_2 purity and the lower the H_2 recovery. Most of the H_2 and CH_4 from the gas phase during the PE steps move from the high-pressure column to the low-pressure column. Therefore, when the PE step numbers are increased, more H_2 and CH_4 are sent to the low-pressure columns, leading to less H_2 being recovered and produced (Fig. 4a) in the CVB but with higher purity (Fig. 4b). For example, when comparing runs 1 (1 PE) and 13 (3 PE), H_2 recovery decreases from 97.46 % to 89.25 %. In contrast, the H_2 purity increases from 41.80 % to 55.87 %, as seen in Table 4. By using 2 PE and P_{vac} lower than or equal to 0.6 bar, it is possible to increase the H_2 concentration from 20 % to up to 50 % with recovery of up to 93 %. These results can be seen in Table 4, in runs 7, 22, and 23.

Fig. 5 illustrates the impact of the number of PE steps and P_{vac} values on productivity and specific energy consumption. When analyzing the effect of vacuum pressure values, we observed a significant change in specific energy consumption (Fig. 5b). At the same time, productivity remained almost unaffected (Fig. 5a). At a deeper vacuum pressure, the higher the specific energy consumption, the higher the productivity. However, when analyzing the impact of PE steps used in the cycle, the productivity decreases while the specific energy consumption increases by increasing the PE steps.

Based on the results for stage 1 presented in Table 4 and shown in Figs. 3, 4, and 5, it was identified that run 7 (2 PE, P_{vac} = 0.2 bar, and t_{ads} = 10 s) provides the best trade-off in terms of H_2 purity (50 %) and recovery (93 %). It is worth noting that while higher H_2 purity could be achieved (60 % H_2 purity in run 15), it led to a substantial drop in H_2 recovery (also around 60 %). In conclusion, stage 1 is used to increase the H_2 concentration from 20 to 50 %, with H_2 recovery of 93 %, and the output data from run 7 was used to design the column for stage 2.

3.3. Stage 2 VPSA performance analysis

The main objective of Stage 2 is to purify H_2 for fuel cell applications (>99.97 %). Thus, a parametric study was conducted in Stage 2 by varying the process variables, such as adsorption time (t_{ads}) and vacuum pressure (P_{vac}). In Stage 2, 3 PEs were used to ensure high H_2 purity and recovery. Each DPE, PPE, and PLP step lasts 5 s. The ADS step varies from 20 to 45 s, and the CVB step time equals the ADS step time.

Stage 2 is fed with the stage 1 product, fixed at 50 % H_2, and a total flowrate of 373 Nm^3/hr. The Stage 2 column properties are summarized in Table 3. The operating conditions and process performance are

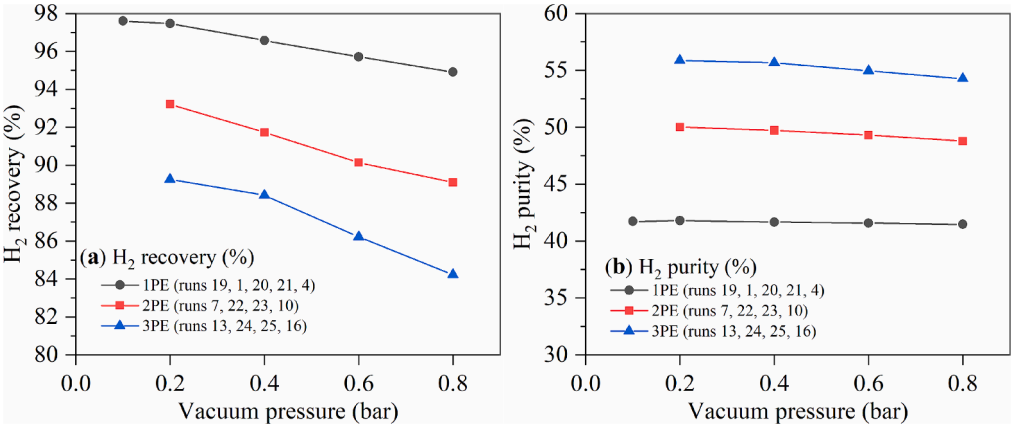

Fig. 4. Effects of P_{vac} and PE step number on the (a) H_2 recovery and (b) purity for the H_2/CH_4 separation in Stage 1. The adsorption time (t_{ads}) was fixed at 10 s.

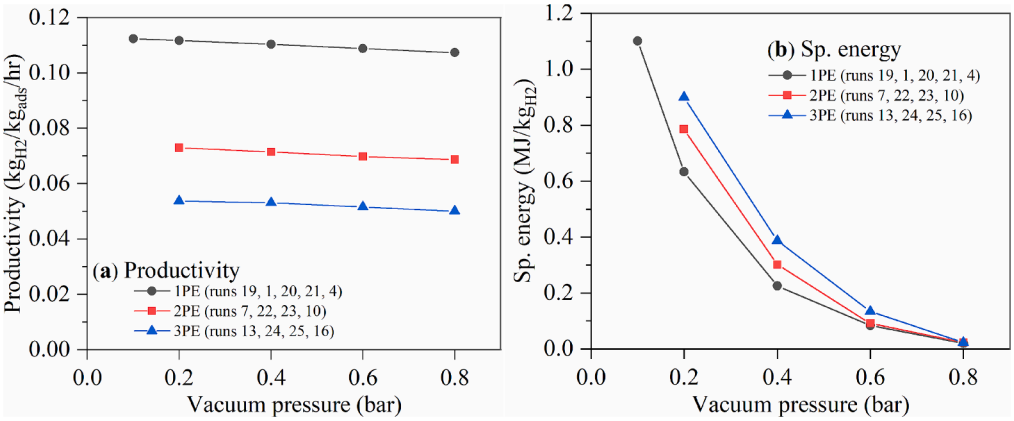

Fig. 5. Effects of P_{vac} and PE step number on the (a) productivity and (b) specific energy for the H_2/CH_4 separation in Stage 1. The adsorption time (t_{ads}) was fixed at 10 s.

ummarized in Table 5. The results are presented for the CSS reached after 250 cycles. The results presented in Table 5 show that Stage 2 can increase the H_2 concentration from 50 % to higher than 99 %, with a recovery rate ranging from 67 to 78 %, as seen in runs 1, 2, and 4. Higher CH_4 recovery is obtained (>90 %) with purity between 88 and 97 %, for example, in runs 2 and 8 shown in Table 5.

Fig. 6 shows the H_2 recovery and purity as a function of vacuum pressure (P_{vac}) and adsorption time (t_{ads}), from where it is possible to see an opposite trend between H_2 recovery (Fig. 6a) and purity (Fig. 6b). The H_2 purity increases while H_2 recovery decreases as P_{vac} decreases. When analyzing the impact of adsorption time, a significant change was observed in both H_2 recovery and purity: higher H_2 recovery and lower H_2 purity for longer adsorption time at the same fixed vacuum pressure. By increasing the adsorption time, CH_4 moves further along the column, displacing H_2 outwards, where it is produced with high recovery and purity. However, CH_4 breaks through the column for longer adsorption time, contaminating the H_2 produced and thus reducing its purity.

Fig. 7 illustrates the impact of the P_{vac} values and adsorption time on productivity and specific energy consumption. A significant change in specific energy consumption was observed (Fig. 7b), while the productivity remained almost unaffected (Fig. 7a). Regarding the effect of the adsorption time, for longer adsorption time, higher productivity and lower specific energy consumption. This is expected since productivity and specific energy consumption are both functions of recovery, as seen in equations (5) and (6). However, productivity directly depends on recovery, while specific energy consumption has an inverse dependence. Thus, higher recovery is achieved, higher productivity, and lower specific energy consumption.

Table 6 summarizes the best result achieved by the dual-stage VPSA to recover H_2 from NGG for fuel cell applications with high purity equal to 99.97 % and recovery over 66 %. The total energy consumption for the vacuum steps, calculated for both stages, is 10.05 MJ/kg_{H2}, which is significantly lower than the values found in the literature, ranging from 16 to 34 MJ/kg_{H2}. Dehdari *et al.* [22] described a dual-stage vacuum swing adsorption (VSA) process using activated carbon (AC) in both stages. When comparing the dual-stage VSA with AC to the proposed process, our system is 37.5 % more economically efficient at the vacuum steps. Moreover, the simulation results indicate that it is possible to produce 1.60×10^{-2} $kg_{H2}/kg_{ads}/hr$, which means 384 $kg_{H2}/ton_{ads}/day$. Stage 2 is responsible for most of the overall energy consumption in the process due to the deepest vacuum pressure and high vacuum step time compared to stage 1. The dual-stage VPSA can also provide H_2 with a purity higher than 99 % for combustion applications with up to 78 % recovery.

4. Conclusions

A dual-stage vacuum pressure swing adsorption (DS-VPSA) process was developed to effectively separate and purify green hydrogen blended in natural gas grids with a low H_2 feed concentration (<20 %). The novelty of the DS-VPSA is the combination of a VPSA filled with a carbon molecular sieve (CMS-3K-172) adsorbent at stage 1 (which kinetically separates H_2 from CH_4), with a VPSA at stage 2 filled with binder-free zeolite 13X with a greater affinity towards CH_4 than H_2. The benefit of using CMS-3K-172 in stage 1 is to retain H_2, which has a lower concentration in the feed (<20 %), instead of retaining CH_4 (conventional PSA cases), which has a higher concentration in the feed (>80 %). A mathematical model was developed in Aspen Adsorption and validated according to data available in the literature to study the best operating conditions of the DS-VPSA through a parametric study. The results showed that DS-VPSA can enrich GH mixed in natural gas grids from 20 % to fuel cell grade requirements (99.97 %) with a recovery of 67 %. The total energy consumption in the vacuum steps for both stages is 37.5 % lower than the values reported in the literature for a dual-stage VSA filled with only one adsorbent (activated carbon [22]). Moreover, the DS-VPSA can also provide H_2 with a purity higher than 99 % for

Table 5
Operating conditions and process performance of the Stage 2 DS-VSA.

Run	t_{ads} (s)	P_{vac} (bar)	H_2 purity (%)	H_2 recovery (%)	CH_4 purity (%)	CH_4 recovery (%)	Sp. Energy (MJ/kg_{H2})	Productivity ($kg_{H2}/kg_{ads}/hr$)
1	20	0.05	99.97	66.94	87.08	99.42	9.27	1.60×10^{-2}
2	20	0.10	99.14	71.65	88.32	99.02	6.28	1.63×10^{-2}
3	20	0.20	94.41	76.57	89.62	93.31	3.63	1.61×10^{-2}
4	30	0.05	99.47	78.34	92.16	99.28	7.81	2.03×10^{-2}
5	30	0.10	97.75	83.35	93.91	97.11	5.23	2.06×10^{-2}
6	30	0.20	91.08	85.94	93.33	90.34	3.00	1.93×10^{-2}
7	45	0.05	97.75	87.26	96.76	97.47	6.50	2.39×10^{-2}
8	45	0.10	94.48	89.12	97.67	92.58	4.29	2.33×10^{-2}
9	45	0.20	86.03	90.45	97.42	81.58	2.40	2.14×10^{-2}

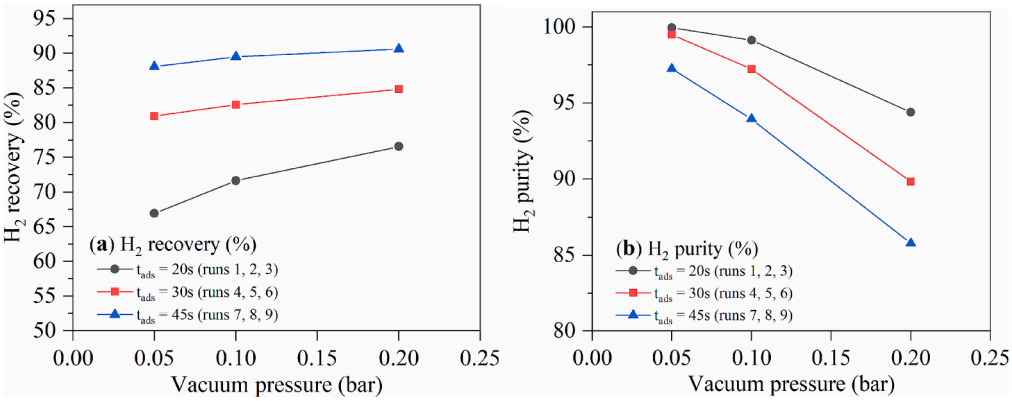

Fig. 6. Effects of P_{vac} and t_{ads} on the (a) H_2 recovery and (b) purity for the H_2/CH_4 separation in Stage 2.

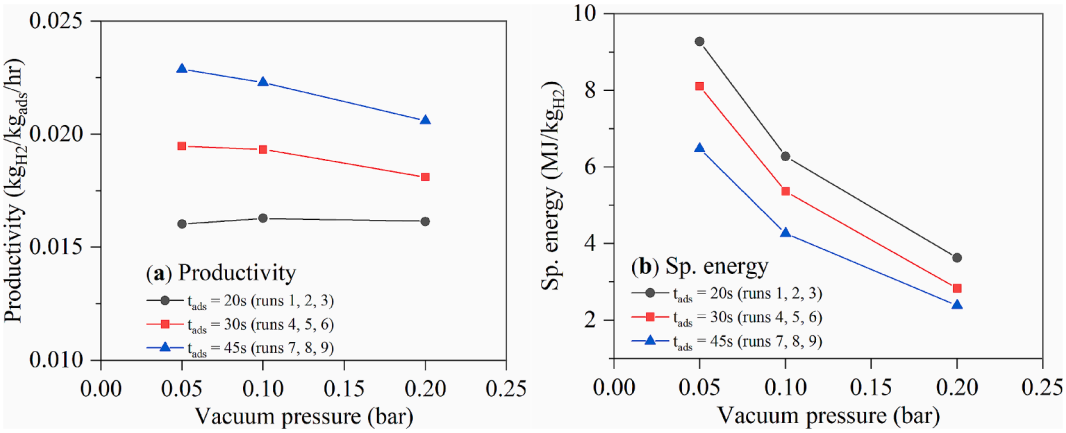

Fig. 7. Effects of P_{vac} and t_{ads} on the (a) productivity and (b) specific energy consumption for the DS-VPSA in Stage 2.

Table 6
Summary of the best performance for the DS-VPSA.

Stage	1 20 % → 50 %	2 50 % → 99.97 %
Feed Flowrate (Nm^3/hr)	1000	373
Product Flowrate (Nm^3/hr)	373	147
P_{ADS} (bar)	30	1
P_{VAC} (bar)	0.20	0.05
H_2 purity (%)	50.03	99.97
H_2 recovery (%)	93.22	66.94
CH_4 purity (%)	98.43	87.08
CH_4 recovery (%)	49.41	99.42
Sp. energy (MJ/kg_{H2})	0.786	9.27
Productivity ($kg_{H2}/kg_{ADS}/hr$)	7.30×10^{-2}	1.60×10^{-2}

combustion applications with up to 78 % recovery. In conclusion, the conceptual DS-VPSA process studied in this work can be a technically viable solution to recover and purify H_2 blended into the natural gas grids.

Declaration of competing interest

The authors declare that they have no known competing financial interests or personal relationships that could have appeared to influence the work reported in this paper.

Acknowledgments

The authors are grateful to the Foundation for Science and Technology (FCT, Portugal) for financial support: (1) under project PTDC/EQU-EPQ/0467/2020 (DOI: 10.54499/PTDC/EQU-EPQ/0467/2020), (2) through the national funds FCT/MCTES (PIDDAC): CIMO, UIDB/00690/2020 (DOI: 10.54499/UIDB/00690/2020) and UIDP/00690/2020 (DOI: 10.54499/UIDP/00690/2020); and SusTEC, LA/P/0007/2020 (DOI:10.54499/LA/P/0007/2020), (3) by the national funds through FCT/MCTES (PIDDAC): LSRE-LCM, UIDB/50020/2020 (DOI: 10.54499/UIDB/50020/2020) and UIDP/50020/2020 (DOI: 10.54499/UIDP/50020/2020); and ALiCE, LA/P/0045/2020 (DOI: 10.54499/LA/P/0045/2020). Additionally, we thank national funding from the FCT Foundation for Science and Technology through the individual research grant 2020.07925.BD (DOI: 10.54499/2020.07925.BD) of Lucas F. A. S. Zafanelli.

Appendix A. Supplementary data

Supplementary data to this article can be found online at https://doi.org/10.1016/j.seppur.2024.130869.

Data availability

Data will be made available on request.

References

[1] Summary for Policymakers, in: C. Intergovernmental Panel on Climate (Ed.) Climate Change 2022 - Mitigation of Climate Change: Working Group III Contribution to the Sixth Assessment Report of the Intergovernmental Panel on Climate Change, Cambridge University Press, Cambridge, 2023, pp. 3-48, https://doi.org/10.1017/9781009157926.001.

[2] J. Sánchez-Laínez, A. Cerezo, M.D. Storch de Gracia, J. Aragón, E. Fernandez, V. Madina, V. Gil, Enabling the injection of hydrogen in high-pressure gas grids:

Investigation of the impact on materials and equipment, Int. J. Hydrogen Energy 52 (2024) 1007–1018, https://doi.org/10.1016/j.ijhydene.2023.05.220.
[3] G. Kakoulaki, I. Kougias, N. Taylor, F. Dolci, J. Moya, A. Jäger-Waldau, Green hydrogen in Europe – A regional assessment: Substituting existing production with electrolysis powered by renewables, Energ. Conver. Manage. 228 (2021) 113649, https://doi.org/10.1016/j.enconman.2020.113649.
[4] W. Liemberger, D. Halmschlager, M. Miltner, M. Harasek, Efficient extraction of hydrogen transported as co-stream in the natural gas grid - The importance of process design, Appl. Energ. 233 (2019) 747–763, https://doi.org/10.1016/j.apenergy.2018.10.047.
[5] L. Dehdari, I. Burgers, P. Xiao, K.G. Li, R. Singh, P.A. Webley, Purification of hydrogen from natural gas/hydrogen pipeline mixtures, Sep. Purif. Technol. 282 (2022) 120094, https://doi.org/10.1016/j.seppur.2021.120094.
[6] J. Yang, L. Dehdari, Y. Guo, J. Guo, R. Singh, P. Xiao, J. Shang, A. Zavabeti, G.K. Li, Hydrogen capture using zeolite 3A for pipeline gas deblending, Chem. Eng. J. 466 (2023) 143224, https://doi.org/10.1016/j.cej.2023.143224.
[7] W. Liemberger, M. Gross, M. Miltner, H. Prazak-Reisinger, M. Harasek, Extraction of Green Hydrogen at Fuel Cell Quality from Mixtures with Natural Gas, Chem. Engineer Trans. 52 (2016) 427–432, https://doi.org/10.3303/CET1652072.
[8] V.I. Agueda, J.A. Delgado, M.A. Uguina, P. Brea, A.I. Spjelkavik, R. Blom, C. Grande, Adsorption and diffusion of H_2, N_2, CO, CH_4 and CO_2 in UTSA-16 metal-organic framework extrudates, Chem. Eng. Sci. 124 (2015) 159–169, https://doi.org/10.1016/j.ces.2014.08.039.
[9] A. Golmakani, S.A. Nabavi, V. Manović, Effect of impurities on ultra-pure hydrogen production by pressure vacuum swing adsorption, J. Ind. Eng. Chem. 82 (2020) 278–289, https://doi.org/10.1016/j.jiec.2019.10.024.
[10] S.-I. Yang, D.-Y. Choi, S.-C. Jang, S.-H. Kim, D.-K. Choi, Hydrogen separation by multi-bed pressure swing adsorption of synthesis gas, Adsorption 14 (2008) 583–590, https://doi.org/10.1007/s10450-008-9133-x.
[11] F. Relvas, R.D. Whitley, C. Silva, A. Mendes, Single-Stage Pressure Swing Adsorption for Producing Fuel Cell Grade Hydrogen, Ind. Eng. Chem. Res. 57 (2018) 5106–5118, https://doi.org/10.1021/acs.iecr.7b05410.
[12] A. Abdeljaoued, F. Relvas, A. Mendes, M.H. Chahbani, Simulation and experimental results of a PSA process for production of hydrogen used in fuel cells, J. Environ. Chem. Eng. 6 (2018) 338–355, https://doi.org/10.1016/j.jece.2017.12.010.
[13] J. Chicano, C.T. Dion, U. Pasaogullari, J.A. Valla, Simulation of 12-bed vacuum pressure-swing adsorption for hydrogen separation from methanol-steam reforming off-gas, Int. J. Hydrogen Energy 46 (2021) 28626–28640, https://doi.org/10.1016/j.ijhydene.2021.06.102.
[14] J. Yang, C.-H. Lee, Adsorption dynamics of a layered bed PSA for H_2 recovery from coke oven gas, AIChE J. 44 (1998) 1325–1334, https://doi.org/10.1002/aic.690440610.
[15] G.D. Marcoberardino, D. Vitali, F. Spinelli, M. Binotti, G. Manzolini, Green hydrogen production from raw biogas: a techno-economic investigation of conventional processes using pressure swing adsorption unit, Processes 6 (2018) 19, https://doi.org/10.3390/pr6030019.
[16] M. Yáñez, F. Relvas, A. Ortiz, D. Gorri, A. Mendes, I. Ortiz, PSA purification of waste hydrogen from ammonia plants to fuel cell grade, Sep. Purif. Technol. 240 (2020) 116334, https://doi.org/10.1016/j.seppur.2019.116334.
[17] M. Nordio, S.A. Wassie, M. Van Sint Annaland, D.A. Pacheco Tanaka, J.L. Viviente Sole, F. Gallucci, Techno-economic evaluation on a hybrid technology for low hydrogen concentration separation and purification from natural gas grid, Int. J. Hydrogen Energy 46 (2021) 23417–23435, https://doi.org/10.1016/j.ijhydene.2020.05.009.
[18] W. Liemberger, M. Gross, M. Miltner, M. Harasek, Experimental analysis of membrane and pressure swing adsorption (PSA) for the hydrogen separation from natural gas, J Clean Prod 167 (2017) 896–907, https://doi.org/10.1016/j.jclepro.2017.08.012.
[19] W. Liemberger, M. Miltner, M. Harasek, Reduced model describing efficient extraction of hydrogen transported as co-stream in the natural gas grid, Comput.-Aided Chem. En. 43 (2018) 1383–1388, https://doi.org/10.1016/B978-0-444-64235-6.50242-4.
[20] I. Burgers, L. Dehdari, P. Xiao, K.G. Li, E. Goetheer, P. Webley, Techno-economic analysis of PSA separation for hydrogen/natural gas mixtures at hydrogen refuelling stations, Int. J. Hydrogen Energy 47 (2022) 36163–36174, https://doi.org/10.1016/j.ijhydene.2022.08.175.
[21] L. Dehdari, P. Xiao, K. Gang Li, R. Singh, P.A. Webley, Separation of hydrogen from methane by vacuum swing adsorption, Chem. Eng. J. 450 (2022) 137911, https://doi.org/10.1016/j.cej.2022.137911.
[22] L. Dehdari, J. Yang, P. Xiao, G.K. Li, P.A. Webley, R. Singh, Separation of hydrogen from 10 % hydrogen + methane mixtures using double-stage Vacuum Swing Adsorption (VSA), Chem. Eng. J. 489 (2024) 151032, https://doi.org/10.1016/j.cej.2024.151032.
[23] L.F.A.S. Zafanelli, E. Aly, A.E. Rodrigues, J.A.C. Silva, A novel cryogenic fixed-bed adsorption apparatus for studying green hydrogen recovery from natural gas grids, Sep. Purif. Technol. 307 (2023) 122824, https://doi.org/10.1016/j.seppur.2022.122824.
[24] L.F.A.S. Zafanelli, E. Aly, A. Henrique, A.E. Rodrigues, G. Mouchaham, J.A.C. Silva, Green hydrogen recovery from natural gas grids by vacuum pressure swing adsorption, Ind. Eng. Chem. Res. 63 (2024) 6333–6346, https://doi.org/10.1021/acs.iecr.3c04532.
[25] S. Cavenati, C.A. Grande, A.E. Rodrigues, Separation of methane and nitrogen by adsorption on carbon molecular sieve, Sep. Sci. Technol. 40 (2005) 2721–2743, https://doi.org/10.1080/01496390500287846.
[26] C.A. Grande, A.E. Rodrigues, Biogas to fuel by vacuum pressure swing adsorption I. Behavior of equilibrium and kinetic-based adsorbents, Indust. Eng. Chem. Res. 46 (2007) 4595–4605, https://doi.org/10.1021/ie061341+.
[27] L.A.M. Rocha, K.A. Andreassen, C.A. Grande, Separation of CO_2/CH_4 using carbon molecular sieve (CMS) at low and high pressure, Chem. Eng. Sci. 164 (2017) 148–157, https://doi.org/10.1016/j.ces.2017.01.071.
[28] D.M. Ruthven, S. Farooq, K.S. Knaebel, Pressure swing adsorption, 1994 VCH Publishers, Inc., New York, 1995.
[29] W.E. Schiesser, G.W. Griffiths, A Compendium of Partial Differential Equation Models: Method of Lines Analysis with Matlab, Cambridge University Press, Cambridge, 2009, https://doi.org/10.1017/CBO9780511576270.
[30] Aspentech, Aspen Adsim 12.1 Adsorption Reference Guide, in, 2020.